Audio Engineering Society

Conference Paper

Presented at the Conference on
Spatial Reproduction
2018 August 6 – 9, Tokyo, Japan

Dataset of near-distance head-related transfer functions calculated using the boundary element method

César D. Salvador[1], Shuichi Sakamoto[1], Jorge Treviño[1], and Yôiti Suzuki[1]

[1]*Research Institute of Electrical Communication (RIEC) and Graduate School of Information Sciences (GSIS), Tohoku University, Sendai 980-8577, Japan*

Correspondence should be addressed to César D. Salvador (salvador@ais.riec.tohoku.ac.jp)

ABSTRACT

The head-related transfer functions (HRTFs) are essential filters used in three-dimensional audio playback devices for personal use. They describe the transmission of sound from a point in space to the eardrums of a listener. Obtaining near-distance HRTFs is important to increase the realism when presenting sounds in the peripersonal space. However, most of the publicly available datasets provide HRTFs for sound sources beyond one meter. We introduce a collection of generic and individual HRTFs for circular and spherical distributions of point sources at distances ranging from 10 cm to 100 cm, spaced 1 cm. The HRTF datasets were calculated using the boundary element method. A sample of the dataset is publicly available in the spatially oriented format for acoustics (SOFA).

1 Introduction

The head-related transfer functions (HRTFs) are linear filters describing the transmission of sound from a point in space to the eardrums of a listener [1, 2, 3]. They describe the acoustic filtering properties of the listener's external anatomical shapes such as their torso, head, and outer ears. The HRTFs contain spatial information used by the listener to locate the source of a sound. They constitute a major tool in spatial sound technology for personal use.

The HRTFs are measured by placing two microphones on the ear canals and loudspeakers around the head [1, 2, 3]. Alternatively, microphones and loudspeakers can be exchanged by virtue of acoustic reciprocity [4, 5]. The HRTFs can also be calculated based on three-dimensional head model acquisition systems and numerical acoustic methods [6, 7, 8, 9, 10, 11, 12, 13]. Publicly available datasets of measured [14, 15, 16, 17, 18, 19] or calculated [18] HRTFs typically contain data for sound sources distributed at a single distance from the center of the head. Such distance is taken on the far field (beyond 1 m) where the HRTFs hardly depend on distance.

Studies on auditory distance perception are highlighting the necessity of obtaining HRTFs for positions within reaching distances to increase the realism during the binaural rendering of sounds in the peripersonal space [20, 21, 22]. However, obtaining near-distance HRTF datasets is still difficult [23, 24, 25, 26, 27, 28].

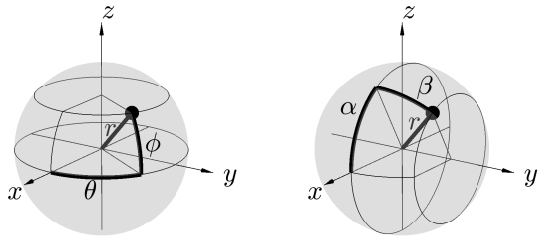

(a) Vertical polar. **(b)** Interaural polar.

Fig. 1: Spherical coordinate systems.

The construction of point sources represents one of the main difficulties encountered during measurements in the near field (within 1 m) [23, 25], whereas the computational power is still a major limitation encountered during calculations involving high resolutions along distance [28].

In this study, we introduce the process for creating a dataset of HRTFs for near-field distances ranging from 10 cm to 100 cm, spaced 1 cm. Some far-field distances are also included (e.g., 150 cm and 200 cm). All HRTFs were calculated by using three-dimensional head models and a numerical solver for the acoustic wave equation running on a scalar-parallel supercomputer. The boundary element method (BEM) [8] was chosen as the numerical solver because it has been validated for point sources in the near field [29]. A sample of the dataset is publicly available* in the spatially oriented format for acoustics (SOFA) [16].

2 Geometry and nomenclature

Figure 1 shows the spherical coordinate systems used in the HRTF dataset to describe positions of point sources around the head. In both coordinate systems, the y-axis is the interaural axis defined by the line connecting the eardrums. The origin of coordinates $\vec{0}$ lies halfway the eardrums and defines the center of the head. The front position lies along the positive x-axis. The $xy-$plane defines the horizontal plane, whereas the $xz-$plane defines the median plane.

In vertical-polar spherical coordinates, a point in space $\vec{x} = (r, \theta, \phi)$ is specified by its radial distance r, azimuth angle $\theta \in [-\pi, \pi]$, and elevation angle $\phi \in [-\frac{\pi}{2}, \frac{\pi}{2}]$. In interaural-polar spherical coordinates, a point in space $\vec{x} = (r, \alpha, \beta)$ is specified by its radial distance r, polar angle $\alpha \in [-\pi, \pi]$, and lateral angle $\beta \in [-\frac{\pi}{2}, \frac{\pi}{2}]$.

The HRTF for the left (or right) ear describes the transmission of sound from a point in space $\vec{x}_{\text{source}}$ to the position of the left (or right) eardrum $\vec{x}_{\text{ear}}$. The free-field HRTF, denoted by H, relates sound pressure P at $\vec{x}_{\text{ear}}$ to the sound pressure P_{ff} that would be measured, using the same sound source, at $\vec{0}$ while the subject is not present. For a given frequency f, the free-field HRTF for a single ear is defined as follows [3]:

$$H(\vec{x}_{\text{ear}}, \vec{x}_{\text{source}}, f) = \frac{P(\vec{x}_{\text{ear}}, \vec{x}_{\text{source}}, f)}{P_{\text{ff}}(\vec{0}, \vec{x}_{\text{source}}, f)}. \quad (1)$$

The interaural HRTF is an important function for the study of interaural cues. It is defined by the ratio between the HRTFs for the left and right ears as follows [3]:

$$H_{\text{interaural}} = \frac{H(\vec{x}_{\text{left ear}}, \vec{x}_{\text{source}}, f)}{H(\vec{x}_{\text{right ear}}, \vec{x}_{\text{source}}, f)}. \quad (2)$$

3 Creating the HRTF dataset

This section describes the process for creating the dataset of near-distance HRTFs. The process comprises head model acquisition, distribution of points around the head, calculation, and storage.

3.1 Head model acquisition

Currently, four models of listeners' heads compose the HRTF dataset reported in this paper: two generic models and two individual models. One generic model was captured by three-dimensional laser scanning, and the other generic model was captured by micro-computerized tomography [8]. The individual models were captured by magnetic resonance imaging.

Figure 2 shows the head models. Panels a and b show the generic models, whereas panels c and d show the individual models. In all panels, the limits of coordinate axes correspond to the smallest parallelepiped containing the head model.

Figure 3 shows examples of interaural HRTFs for the head models in Fig 2. All plots consider point source distances ranging from 10 cm to 100 cm, spaced 1 cm, along azimuth $\theta = 100^\circ$ and elevation $\phi = 20^\circ$. As the point source approaches the left ear, the individual dependencies are more noticeable because the acoustic shadow effect of the head becomes more prominent.

*http://www.ais.riec.tohoku.ac.jp/~salvador/download.html

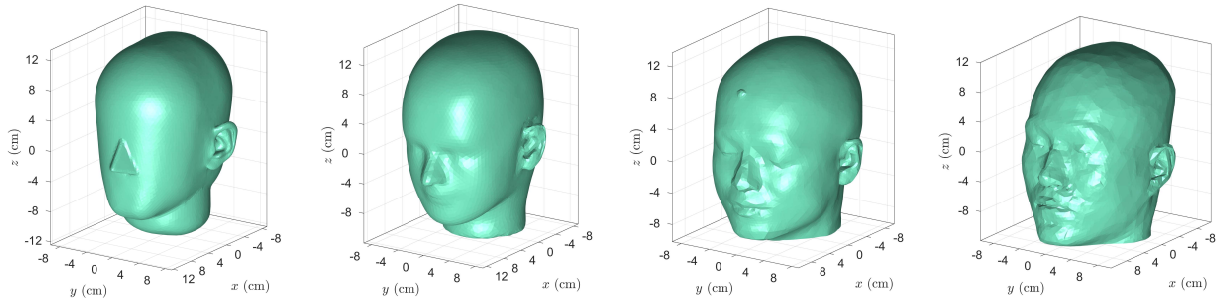

(a) Head 1. **(b)** Head 2. **(c)** Head 3. **(d)** Head 4.

Fig. 2: Generic (left) and individual (right) head models.

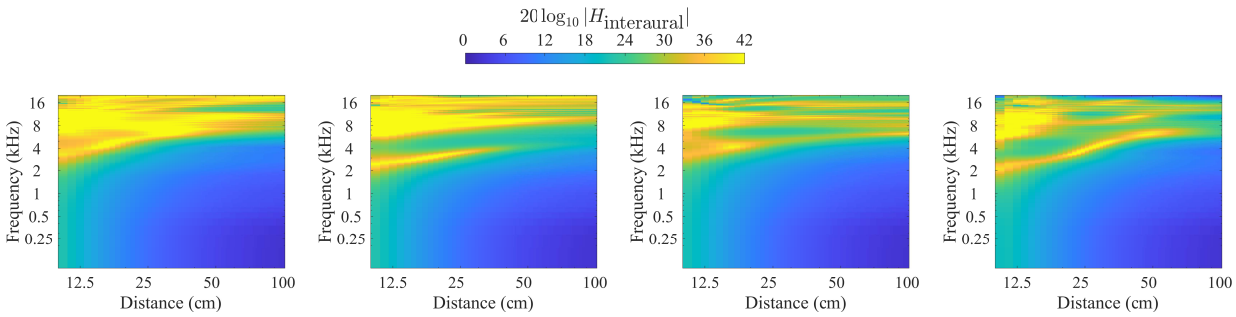

(a) Head 1. **(b)** Head 2. **(c)** Head 3. **(d)** Head 4.

Fig. 3: Interaural HRTFs for a distribution of sources along distances at azimuth $\theta = 100°$ and elevation $\phi = 20°$.

3.2 Distributing points around the head

The choice of suitable distributions of point sources along directions is also an important issue in HRTF applications such as the analysis and extraction of spatiospectral acoustic features [30], the interpolation along angles [31, 32], and the extrapolation along distance [33, 34]. These applications often require the analysis of acoustic data in transform domains defined by the Fourier transform along circular [34] and spherical boundaries [35].

In this study, the grids used to distribute the sources around the head have been selected so as to ensure the accurate computation of Fourier transforms over circular and spherical grids. For each head model and each distance, the dataset contains two types of circular grids and four types of spherical grids.

Circular grids are described in vertical-polar spherical coordinates. The point sources are equiangularly spaced 1°. The circular grids used in the dataset are of the following two types:

- Horizontal-plane, circular grids
- Median-plane, circular grids.

Panels (a) and (b) in Fig. 4 respectively show examples of horizontal-plane and median-plane distributions for a single distance.

Spherical, equiangular grids enable the accurate computation of Fourier transforms on circular boundaries. According to the coordinate system underlying their definition, the following two types of spherical grids were considered:

- Vertical-polar, equiangular, spherical grids
- Interaural-polar, equiangular, spherical grids.

The use of vertical-polar, spherical coordinates is convenient to describe distributions without points over the south polar cap region of the sphere [36]. The use of interaural-polar, spherical coordinates is important in studies of binaural localization along the so-called cones of confusion [14]. Panels (a) and (b) in Fig. 5 respectively show examples of vertical-polar and interaural-polar distributions for a single distance.

Spherical, nearly-uniform grids enable the accurate computation of Fourier transforms on spherical boundaries. According to the method used to distribute points on the whole sphere, the two following types of spherical grids were considered:

- Icosahedral, spherical grids
- Maximum-determinant, spherical grids.

Icosahedral, spherical grids are constructed by subdivision of the icosahedron's edges [37]. Maximum-determinant, spherical grids are based on the maximum-determinant criteria for precise integration on spherical surfaces [38].

3.3 Calculation and storage of HRTFs

HRTF calculation was performed in the frequency domain using the BEM Solver in [8]. The BEM solver runs on the scalar-parallel supercomputer of the Cyberscience Center, Tohoku University, which consists of 68 nodes of type LX 406-Re2[†].

Calculated datasets were stored as free-field head-related impulses responses (HRIRs) in the time domain by using the SOFA format [16]. In addition, the corresponding metadata containing information such as the underlying geometry and simulation conditions was also included in the SOFA file.

4 Reading SOFA files in Matlab

The SOFA files corresponding to circular and spherical HRTF datasets for one of the individual models have been made publicly available (see footnote on page 2). Accessing the data requires MATLAB or GNU Octave. In addition, it is necessary to install the SOFA Matlab/Octave API version 1.0.2 [16]. A Matlab script example to read the SOFA file containing a horizontal-plane, circular dataset and its metadata is described in Table 1. The script also performs a distance variation analysis detailed in the next section.

[†] http://www.cc.tohoku.ac.jp/data/pamphlet_en.pdf

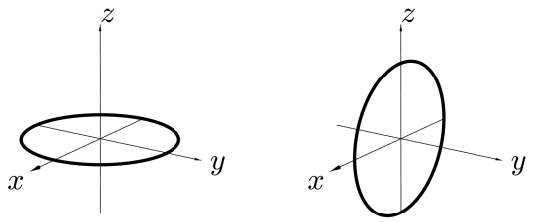

(a) Horizontal plane. **(b)** Median plane.

Fig. 4: Circular distributions of point sources.

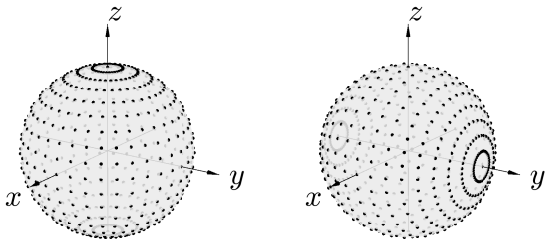

(a) Vertical polar. **(b)** Interaural polar.

Fig. 5: Equiangular, spherical distributions.

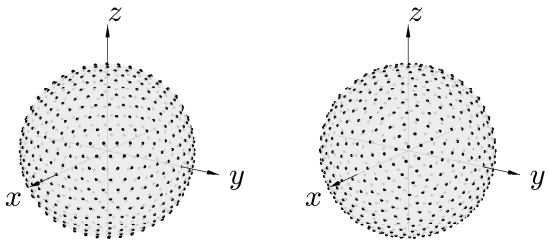

(a) Icosahedral. **(b)** Maximum determinant.

Fig. 6: Nearly-uniform, spherical distributions.

5 Distance variation analyses

The near-distance HRTF datasets created in this study can be used to investigate the variations over distance by means of modal analyses on angular domains as proposed in [34]. Modal analyses consist on examining the ratio of angular Fourier representations between an initial distance r_1 and a final distance r_2, such that $r_1 > r_2$. Such a kind of analysis is convenient to unmask

Table 1: Matlab script that reads a circular dataset and its metadata to perform a distance variation analysis.

```
%% Start SOFA Matlab/Octave API
SOFAstart;

%% Read structure array Obj from SOFA file
Obj = SOFAload('gen01_h_circ_hor_dir360_dist141.sofa');
Obj = orderfields(Obj);

%% Dimensions of data
Fs = Obj.Data.SamplingRate;                 % sampling frequency in Hertz
Ns = Obj.API.N;                             % number of samples along time
sample_circshift = Obj.Data.Delay;          % circular delay of HRIRs
Nazim = Obj.SourcePositionNumberAzimuths;   % number of source azimuths
Nelev = Obj.SourcePositionNumberElevations; % number of source elevations
Ndir = Obj.SourcePositionNumberDirections;  % number of source directions
Ndist = Obj.SourcePositionNumberDistances;  % number of source distances
Npos = Obj.API.M;                           % number of source positions (Ndir*Ndist)
c = Obj.SpeedOfSoundInMPS;                  % speed of sound in air (m/s)

%% Head-related impulse responses (size: Ns * Ndir * Ndist * Nh)
head_model_name = Obj.GLOBAL_ListenerShortName;
HRIR_left = permute(reshape(squeeze(Obj.Data.IR(:,1,:)), [Ndir Ndist Ns]), [3 1 2]);
HRIR_right = permute(reshape(squeeze(Obj.Data.IR(:,2,:)), [Ndir Ndist Ns]), [3 1 2]);

%% One-dimensional domains
t = (0:Ns-1)*1/Fs;                          % time (seconds)
f = (0:Ns/2)*Fs/Ns;                         % frequency (Hertz)
m = -Nazim/2:Nazim/2-1;                     % circular harmonics domain

%% Source positions in spherical and Cartesian coordinates
azim = Obj.SourcePosition(:, 1);
elev = Obj.SourcePosition(:, 2);
dist = Obj.SourcePosition(:, 3);
[x(:, 1), x(:, 2), x(:, 3)] = sph2cart(azim*pi/180, elev*pi/180, dist);
x = reshape(x, [Ndir Ndist 3]);             % Cartesian in m (size: Ndir*Ndist*3)

%% Head-related transfer functions (size: Ns/2+1 * Ndir * Ndist)
HRTF_left = fft(HRIR_left); HRTF_left = HRTF_left(1:Ns/2+1, :, :);
HRTF_right = fft(HRIR_right); HRTF_right = HRTF_right(1:Ns/2+1, :, :);
HRTF_interaural = HRTF_left./HRTF_right;

% Initial distance in meters
dist_init = 1; ind_dist_init = find(dist(1, :) == dist_init); Ndist = ind_dist_init;

% Initial and final distance HRTFs
HRTF_left_initial = squeeze(HRTF_left(:, :, ind_dist_init));
HRTF_right_initial = squeeze(HRTF_right(:, :, ind_dist_init));
HRTF_left_final = squeeze(HRTF_left(:, :, 1:ind_dist_init));
HRTF_right_final = squeeze(HRTF_right(:, :, 1:ind_dist_init));

%% Circular Fourier analysis of distance variation for the left ear (Dm)
HRTF_left_initial_m = fftshift(fft(fftshift(HRTF_left_initial, 2), [], 2), 2);
HRTF_left_initial_m = repmat(HRTF_left_initial_m, [1 1 Ndist]);

HRTF_left_final = permute(HRTF_left_final, [1 3 2]);
HRTF_left_final = reshape(HRTF_left_final, [(Ns/2+1)*Ndist Ndir]);
HRTF_left_final_m = fftshift(fft(fftshift(HRTF_left_final, 2), [], 2), 2);
HRTF_left_final_m = reshape(HRTF_left_final_m, [(Ns/2+1) Ndist Ndir]);
HRTF_left_final_m = permute(HRTF_left_final_m, [1 3 2]);

D_initial_to_final_left_m = HRTF_left_final_m ./ HRTF_left_initial_m;
```

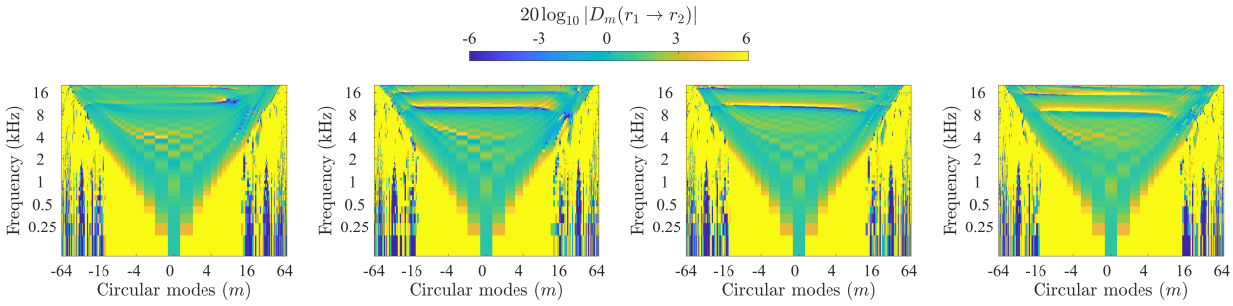

(a) Head 1. **(b)** Head 2. **(c)** Head 3. **(d)** Head 4.

Fig. 7: Fourier analysis of distance variation between two horizontal circles, from $r_1 = 100$ cm to $r_2 = 25$ cm.

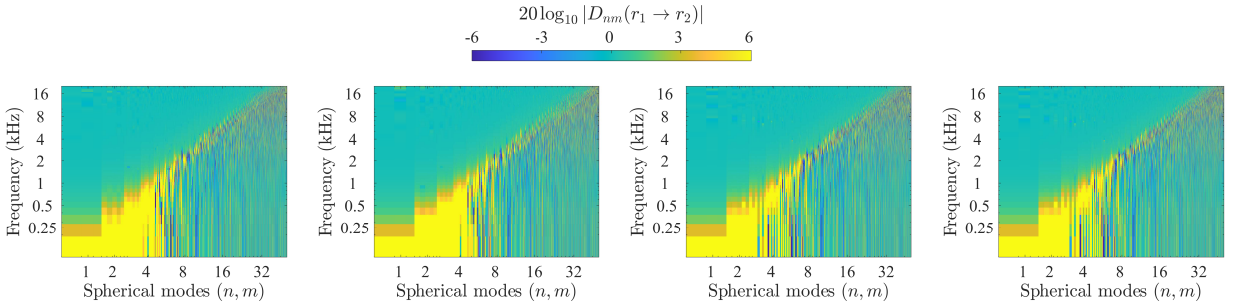

(a) Head 1. **(b)** Head 2. **(c)** Head 3. **(d)** Head 4.

Fig. 8: Fourier analysis of distance variation between two spherical surfaces, from $r_1 = 100$ cm to $r_2 = 25$ cm.

patterns of distance variation that would otherwise be hardly observed in the natural angular domain.

Distance variation in the circular Fourier domain is performed based on the following expression:

$$D_m(r_1 \to r_2) = \frac{\int_{\theta=-\pi}^{\pi} H(r_2,\theta)\exp(jm\theta)d\theta}{\int_{\theta=-\pi}^{\pi} H(r_1,\theta)\exp(jm\theta)d\theta}, \quad (3)$$

where m represents the index to circular modes.

Figure 7 shows examples of D_m in (3) for the horizontal-plane, circular datasets of the head models in Fig 2. Distance variation mainly emerges as a symmetric angular bandwidth that increases with increasing frequency. Within the angular bandwidth of interest, it can be observed that individual-dependent features are more prominent at middle and higher frequencies.

Distance variation in the spherical Fourier domain is performed by using the following expression:

$$D_{nm}(r_1 \to r_2) = \frac{\int_{\Omega\in\mathbb{S}^2} H(r_2,\Omega)Y_n^m(\Omega)d\Omega}{\int_{\Omega\in\mathbb{S}^2} H(r_1,\Omega)Y_n^m(\Omega)d\Omega}, \quad (4)$$

where $\Omega = (\theta,\phi)$, $d\Omega = \cos\phi d\phi d\theta$, and Y_n^m is the fully-normalized spherical harmonic function of order n and degree m defined in [39].

Figure 8 shows examples of D_{nm} in (4) for the maximum-determinant, spherical datasets of the head models in Fig 2. Distance variation is mainly displayed as an angular bandwidth that increases towards the higher modes with increasing frequency. Individual-dependent features are hardly observed within the angular bandwidth of interest, as opposed to the results from circular modal analyses shown in Fig. 7.

In addition, the above analyses suggest that the modeling of far-to-near distance variation, both on the circle and on the sphere, is a difficult process that requires low-frequency boosting of high modes. This observation is in agreement with the ill-conditioned nature of the acoustic propagation problem [39]. Moreover, ill-conditioning particularly constitutes a major difficulty when designing distance-varying filters for the synthesis of HRTFs on the horizontal plane from their values on circular boundaries [34].

6 Summary

The process for creating a collection of generic and individual head-related transfer functions (HRTFs), for circular and spherical distributions of point sources at near distances from the head, was presented. The HRTF datasets were calculated using a boundary element method (BEM) solver that has been validated for near distances. Dense distributions of points were considered thanks to the availability of a parallel supercomputer system. Distance variation analyses on circular and spherical Fourier domains were also presented to exemplify individual dependencies of HRTFs along distance. A sample of the dataset was made publicly available in the SOFA format. There are plans to include more models and gradually integrate the calculated HRTFs into the Research Institute of Electrical Communication (RIEC) HRTF dataset [17].

Acknowledgment

This work was supported by the JSPS Grant-in-Aid for Scientific Research no. JP16H01736 and no. JP17K12708.

References

[1] M. Morimoto, Y. Ando, Z. Maekawa, On head-related transfer function in distance perception, in: Proc. Congress Acoust. Soc. Jpn., Japan, 1975, pp. 137–138, (in Japanese).

[2] H. Møller, Fundamentals of binaural technology, Appl. Acoust. 36 (3-4) (1992) 171–218. doi:10.1016/0003-682X(92)90046-U.

[3] J. Blauert, Spatial hearing: The psychophysics of human sound localization, revised Edition, MIT Press, Cambridge, MA, USA; London, England., 1997.

[4] D. N. Zotkin, R. Duraiswami, E. Grassi, N. A. Gumerov, Fast head-related transfer function measurement via reciprocity, J. Acoust. Soc. Am. 120 (4) (2006) 2202–2215. doi:10.1121/1.2207578.

[5] N. Matsunaga, T. Hirahara, Issues of the HRTFs measurement via reciprocal method, Tech. Rep. IEICE. EA 109 (240) (2009) 107–112.

[6] B. F. G. Katz, Boundary element method calculation of individual head-related transfer function. I. Rigid model calculation, J. Acoust. Soc. Am. 110 (5) (2001) 2440–2448. doi:10.1121/1.1412440.

[7] B. F. G. Katz, Boundary element method calculation of individual head-related transfer function. II. Impedance effects and comparisons to real measurements, J. Acoust. Soc. Am. 110 (5) (2001) 2449–2455. doi:10.1121/1.1412441.

[8] M. Otani, S. Ise, Fast calculation system specialized for head-related transfer function based on boundary element method, J. Acoust. Soc. Am. 119 (5) (2006) 2589–2598. doi:10.1121/1.2191608.

[9] P. Mokhtari, H. Takemoto, R. Nishimura, H. Kato, Comparison of simulated and measured HRTFs: FDTD simulation using MRI head data, in: AES 123 Convention, 2007.

[10] K. Matsui, A. Ando, Estimation of individualized head-related transfer function based on principal component analysis, Acoust. Sci. Technol. 30 (5) (2009) 338–347. doi:10.1250/ast.30.338.

[11] N. A. Gumerov, A. E. O'Donovan, R. Duraiswami, D. N. Zotkin, Computation of the head-related transfer function via the fast multipole accelerated boundary element method and its spherical harmonic representation, J. Acoust. Soc. Am. 127 (1) (2010) 370–386.

[12] A. Meshram, R. Mehra, D. Manocha, Efficient HRTF computation using adaptive rectangular decomposition, in: AES 55th Int. conf. Spatial Audio, 2014.

[13] H. Ziegelwanger, P. Majdak, W. Kreuzer, Numerical calculation of listener-specific head-related transfer functions and sound localization: Microphone model and mesh discretization, J. Acoust. Soc. Am. 138 (1) (2015) 208–222. doi:10.1121/1.4922518.

[14] V. Algazi, R. Duda, D. Thompson, C. Avendano, The CIPIC HRTF database, in: Proc. IEEE WASPAA, 2001, pp. 99–102. doi:10.1109/ASPAA.2001.969552.

URL http://interface.cipic.ucdavis.edu/sound/hrtf.html

[15] S. Takane, D. Arai, T. Miyajima, K. Watanabe, Y. Suzuki, T. Sone, A database of head-related transfer functions in whole directions on upper hemisphere, Acoust. Sci. Technol. 23 (3) (2002) 160–162. doi:10.1250/ast.23.160.

[16] P. Majdak, Y. Iwaya, T. Carpentier, R. Nicol, M. Parmentier, A. Roginska, Y. Suzuki, K. Watanabe, H. Wierstorf, H. Ziegelwanger, M. Noisternig, Spatially oriented format for acoustics: a data exchange format representing head-related transfer functions, in: AES 134 Convention, 2013.
URL https://www.sofaconventions.org/

[17] K. Watanabe, Y. Iwaya, Y. Suzuki, S. Takane, S. Sato, Dataset of head-related transfer functions measured with a circular loudspeaker array, Acoust. Sci. Technol. 35 (3) (2014) 159–165. doi:10.1250/ast.35.159.
URL http://www.riec.tohoku.ac.jp/pub/hrtf/index.html

[18] C. T. Jin, P. Guillon, N. Epain, R. Zolfaghari, A. v. Schaik, A. I. Tew, C. Hetherington, J. Thorpe, Creating the Sydney York morphological and acoustic recordings of ears database, IEEE Trans. Multimedia 16 (1) (2014) 37–46. doi:10.1109/TMM.2013.2282134.

[19] F. Brinkmann, The FABIAN head-related transfer function data base, Tech. rep. (2017).
URL http://dx.doi.org/10.14279/depositonce-5718

[20] D. S. Brungart, W. M. Rabinowitz, Auditory localization of nearby sources. Head-related transfer functions, J. Acoust. Soc. Am. 106 (3) (1999) 1465–1479. doi:10.1121/1.427180.

[21] D. S. Brungart, Near-Field Virtual Audio Displays, Presence: Teleop. Virt. Env. 11 (1) (2002) 93–106. doi:10.1162/105474602317343686.

[22] G. Parseihian, C. Jouffrais, B. F. G. Katz, Reaching nearby sources: comparison between real and virtual sound and visual targets., Front. Neurosci. 8 (269). doi:10.3389/fnins.2014.00269.

[23] T. Qu, Z. Xiao, M. Gong, Y. Huang, X. Li, X. Wu, Distance-dependent head-related transfer functions neasured with high spatial resolution using a spark gap, IEEE Trans. Audio, Speech, Language Process. 17 (6) (2009) 1124–1132. doi:10.1109/TASL.2009.2020532.

[24] B. Xie, X. Zhong, G. Yu, S. Guan, D. Rao, Z. Liang, C. Zhang, Report on research projects on head-related transfer functions and virtual auditory displays in China, J. Audio Eng. Soc. 61 (5) (2013) 314–326.
URL http://www.aes.org/e-lib/browse.cfm?elib=16826

[25] H. Wierstorf, M. Geier, A. Raake, S. Spors, A free database of head-related impulse response measurements in the horizontal plane with multiple distances, in: AES 130 Convention, London, UK, 2011.

[26] C. Pörschmann, J. M. Arend, A. Neidhardt, A spherical near-field HRTF set for auralization and psychoacoustic research, in: Proc. 142 Audio Eng. Soc. Convention, 2017.
URL http://www.aes.org/e-lib/browse.cfm?elib=18697

[27] G. Yu, R. Wu, Y. Liu, B. Xie, Near-field head-related transfer-function measurement and database of human subjects, J. Acoust. Soc. Am. 143 (3) (2018) EL194–EL198. doi:10.1121/1.5027019.

[28] Y. Rui, G. Yu, B. Xie, Y. Liu, Calculation of individualized near-field head-related transfer function database using boundary element method, in: Proc. 134th Convention Audio Eng. Soc., 2013.
URL http://www.aes.org/e-lib/browse.cfm?elib=16801

[29] M. Otani, T. Hirahara, Numerical study on source-distance dependency of head-related transfer functions, J. Acoust. Soc. Am. 125 (5) (2009) 3253–3261. doi:10.1121/1.3111860.

[30] S. Spagnol, M. Geronazzo, F. Avanzini, On the Relation Between Pinna Reflection Patterns and

Head-Related Transfer Function Features, Audio, Speech, and Language Processing, IEEE Transactions on 21 (3) (2013) 508–519. doi:10.1109/TASL.2012.2227730.

[31] M. J. Evans, Analyzing head-related transfer functions measurements using surface spherical harmonics, J. Acoust. Soc. Am. 104 (4) (1998) 2400–2411.

[32] Y. Hu, J. Lu, X. Qiu, Direction of arrival estimation of multiple acoustic sources using a maximum likelihood method in the spherical harmonic domain, Appl. Acoust. 135 (2018) 85 – 90. doi:10.1016/j.apacoust.2018.02.005.

[33] R. Duraiswami, D. N. Zotkin, N. A. Gumerov, Interpolation and range extrapolation of HRTFs, in: Proc. IEEE ICASSP, Vol. 4, 2004, pp. 45–48. doi:10.1109/ICASSP.2004.1326759.

[34] C. D. Salvador, S. Sakamoto, J. Treviño, Y. Suzuki, Distance-varying filters to synthesize head-related transfer functions in the horizontal plane from circular boundary values, Acoust. Sci. Technol. 38 (1) (2017) 1–13. doi:10.1250/ast.38.1.

[35] C. D. Salvador, S. Sakamoto, J. Treviño, Y. Suzuki, Boundary matching filters for spherical microphone and loudspeaker arrays, IEEE/ACM Trans. Audio, Speech, Language Process. 26 (3) (2018) 461–474. doi:10.1109/TASLP.2017.2778562.

[36] A. Bates, Z. Khalid, R. Kennedy, Novel sampling scheme on the sphere for head-related transfer function measurements, IEEE/ACM Trans. Audio, Speech, Language Process. 23 (6) (2015) 1068–1081. doi:10.1109/TASLP.2015.2419971.

[37] R. Sadourny, A. Arakawa, Y. Mintz, Integration of the nondivergent barotropic vorticity equation with an icosahedral-hexagonal grid for the sphere 1, Mon. Wea. Rev. 96 (6) (1968) 351–356. doi:http://dx.doi.org/10.1175/1520-0493(1968)096<0351:IOTNBV>2.0.CO;2.

[38] R. S. Womersley, I. H. Sloan, How good can polynomial interpolation on the sphere be?, Adv. Comput. Math. 14 (2001) 195–226.

[39] E. G. Williams, Fourier Acoustics: Sound Radiation and Nearfield Acoustical Holography, Academic Press, London, UK, 1999.